

available at [www.sciencedirect.com](http://www.sciencedirect.com)journal homepage: [www.elsevier.com/locate/carbon](http://www.elsevier.com/locate/carbon)

# Chemical and electrochemical ageing of carbon materials used in supercapacitor electrodes

M. Zhu<sup>a,b</sup>, C.J. Weber<sup>c</sup>, Y. Yang<sup>a,d</sup>, M. Konuma<sup>a</sup>, U. Starke<sup>a</sup>, K. Kern<sup>a</sup>, A.M. Bittner<sup>a,\*</sup>

<sup>a</sup>Max Planck Institute for Solid State Research, Heisenbergstr. 1, D-70569 Stuttgart, Germany

<sup>b</sup>Merck China, Chemical Technology Office, Shanghai, PR China

<sup>c</sup>Freudenberg Vliesstoffe KG, Weinheim, Germany

<sup>d</sup>University of California, Irvine, CA 92697, USA

## ARTICLE INFO

### Article history:

Received 15 October 2007

Accepted 20 July 2008

Available online 31 July 2008

## ABSTRACT

Electrochemical double layer capacitors–supercapacitors–are usually based on highly porous activated carbon electrodes. The chemical and electrochemical inertness of carbon assures a very long lifetime. However, on the timescale of months the capacitors slowly lose some capacitance, and the equivalent series resistance rises. This “ageing” is faster when temperature and operation voltage are increased. To elucidate ageing processes in the electrodes, we analyzed aged samples of activated carbon, and also of carbon black, which is used as conductive additive. The experimental methods were infrared, Raman, and photoelectron spectroscopy, and nitrogen porosimetry. The electrodes are not completely inert, and their ageing is due to chemical and electrochemical reactions at the carbon. Moreover, the ageing procedures are much stronger at the positive pole. We found that oxygen, hydrogen, nitrogen, and fluorine, which originate from trace water and from the electrolyte, can covalently attach to the electrodes and form various chemical groups (e.g. OH, COOH, CONH, and F).

© 2008 Elsevier Ltd. All rights reserved.

## 1. Introduction

Supercapacitors are becoming more and more popular because they can improve the performance of electrolytic capacitors in terms of specific energy, and that of rechargeable batteries in terms of specific power. In addition, supercapacitors have a much longer cycle life than batteries because no or negligibly small chemical charge transfer reactions are involved. With these properties, they are of key importance in supporting the voltage of a system during increased loads for many devices, from portable equipment to hybrid electric vehicles, passenger cars, buses, and locomotives. Examples for exploiting the high specific power are engine starting and acceleration. Due to the nearly symmetrical behavior for charging and discharging, supercapacitors are suitable

for regenerative braking, which means they can recuperate the otherwise lost energy during slowing down and braking. The long cycle life is a key feature. In addition, applications in electronic devices such as cellular phones, camcorders and navigation devices, for low drain-rate memory, and for microprocessor and real time clock backup, are all based on the long life [1,2]. We here show that a multimethod physicochemical analysis provides important criteria and data to select carbon materials for electrode fabrication, especially as measure against ageing. Moreover, our results suggest that a simple desktop infrared spectrometer might suffice for selecting the desired material.

One of the biggest drawbacks for a wider use of supercapacitors is that—under critical conditions, like high temperature or over(dis)charge—irreversible electrochemical processes can

\* Corresponding author: Fax: +49 711 689 1662.

E-mail address: [a.bittner@fkf.mpg.de](mailto:a.bittner@fkf.mpg.de) (A.M. Bittner).

0008-6223/\$ - see front matter © 2008 Elsevier Ltd. All rights reserved.

doi:10.1016/j.carbon.2008.07.025

occur [3,4] and result in ageing processes, especially capacitance loss and increase of the equivalent series resistance. This will obviously influence the performance (slower charging/discharging), and the long term stability of the system. It is therefore important to investigate the ageing mechanisms for further improvement and development. From the electrochemical characteristics, one can expect synthesis and deposition of unwanted substances on electrode surfaces, or gas evolution, all from decomposition of the electrolyte (tetraethylammonium tetrafluoroborate,  $(C_2H_5)_4N^+ BF_4^-$ , in acetonitrile,  $CH_3CN$ ). Such electrolyte-based ageing processes influence the performance to various degrees: First, the active element in the system is irreversibly consumed (presumably of minor relevance since not much material is lost); second, gas evolution [5] and accumulation in the closed systems increase the internal pressure, which can be a safety issue. However, also the carbon materials used in the electrodes are affected, [3,4] and all the structural and chemical characteristics of the electrodes change, which in turn influences capacitance and equivalent series resistance (although also other components such as the separator or the casing or the electrolyte [5] may cause ageing). The overall process is somewhat comparable to the formation of the solid-electrolyte interphase in lithium ion batteries [6].

We here focus solely on the electrodes, which make up a large part of the capacitor device volume. The electrodes are simplified by using only activated carbon powder, without additives such as binders or conductive agents. We elucidated slow chemical and physical processes that cause ageing of the carbon materials on the scale of months, by either polarizing activated carbon powder electrodes at 25 °C, or by immersing them in electrolyte at 50 °C. Our aim is establishing a simple model system, but at the same time staying as close as possible to typical production conditions. For this reason, we mostly used only 80 °C as drying temperature, thereby not removing all water traces. For comparison, and to elucidate a possible role in ageing, we also tested carbon black, which is used as conductive additive to keep the equivalent series resistance and thus the charging time as small as possible.

### 1.1. Activated carbon as main element in supercapacitor electrodes

Activated carbon is utilized as active ingredient in supercapacitors to provide the capacitance, mainly because its internal surface area can be very high, and because it is very cheap and lightweight, compared to alternatives such as carbon tubes or porous noble metals. Activated carbon can be obtained from a wide variety of natural sources. However, it is not easy to control the extent and size distribution of the resulting pores. Synthetic resins and other polymeric materials can offer better defined activated carbons. Note that also the activating agent and the conditions of the activation process determine the characteristics of the final product [7]. While graphene sheets make up a large part of activated carbon, the exact structure, especially of the pores, and the details of the carbon chemistry, are complex. Small graphitic crystallites of only a few atomic planes [8] are crosslinked by partially  $sp^3$ -bonded carbon units [9]. Recent models based on TEM and X-ray scattering data shift the focus even further

to crosslinks, away from the extremely small graphitic crystallites [10].

### 1.2. Carbon black as conductive agent in supercapacitor electrodes

Carbon black is electrically conductive and is widely applied for conductivity improvement in polymer engineering and electrochemical industry. It is composed of more or less spherical particles (primary particles) with diameters in the size range of 10–75 nm, which form aggregates (fused primary particles) of 50–400 nm size. When homogeneously dispersed and mixed with the matrix (for supercapacitors activated carbon, binders [11] and possibly additives), the aggregates form a compact one-, two- or three-dimensional network of the conducting phase. Carbon black is usually very pure (ca. 97–99% C) and is considered to be “amorphous”. However, the microstructure is similar to that of graphite.

## 2. Experimental methods (see Supporting information)

For each type of carbon we selected three samples from various sources. Two activated carbons (A and B) stem from natural precursors (coconut shell), and one (C) from synthetic resin. The conductive agents are one acetylene carbon black sample (A-B), and two Ketjen blacks, Ketjen black A (K-A) and Ketjen black B (K-B). For pure “chemical ageing”, powder samples were dried in vacuum at 80 °C and handled in an argon flowbox (<30 ppm water). They were immersed in electrolyte, and stored at 50 °C. Once a month samples were taken and carefully rinsed with acetonitrile. For electrochemical ageing, activated carbon powder samples were assembled in the flowbox in steel electrode cells (Supporting information). Different from supercapacitors, no binders or conductive agents were used, only paper (stored in the flowbox) as separator. The cells were polarized at  $2.9 \pm 0.1$  V for 45 days (the negligible current flow allowed to use a simple voltage source, whose low accuracy is much less important than the ageing temperature, especially in actual devices). Upon emersion, the powder samples were rinsed with acetonitrile and dried at 60 °C in air and at 80 °C in vacuum. The experimental procedure for the conductive agents was identical.

Nitrogen adsorption was measured at  $-196$  °C with an Autosorb-1 porosimeter (Quantachrome) after >18 h outgassing at 150 °C. The specific surface area was calculated by the five point BET method in the range from  $P/P_0 = 0.01$  to 0.1. Calculations with various models were carried out with the Autosorb® Software. CHN (carbon, nitrogen, hydrogen) elemental analysis was performed with a Perkin Elmer Analyzer 240 at Universität Stuttgart. The samples were rinsed and dried in vacuum at 80 °C before the measurement.

Raman spectra were obtained in backscattering geometry with a Labram 010 spectrometer (Jobin Yvon Horiba, France) under 632.8 nm excitation. Powder samples were pressed onto microscope slides. Infrared spectra were collected on an Equinox 55 spectrometer (Bruker) under Attenuated Total Reflection (ATR) with a germanium crystal as the internal reflection element (PIKE Miracle). All spectra were referenced to the raw spectrum of air. X-ray Photoelectron Spectroscopy

(XPS) characterization was carried out with an AXIS Ultra spectrometer (Kratos) with Al K $\alpha$  radiation. The powders were pressed on an indium foil and ion-sputtered to remove the topmost ~20 nm of material.

### 3. Results for activated carbon

We worked with three samples of activated carbons with comparable BET (Brunauer–Emmett–Teller) surfaces: Samples A and B from natural precursors (coconut shell), and carbon C from synthetic resin. Note that so-called “chemical ageing” experiments refer to heating samples in electrolyte for at least one month, while the usual electrochemical ageing is polarization at 2.9 V. Whenever it is appropriate, we will compare our results to electrical performance data of Epcos ultracaps.

#### 3.1. Microstructural changes in activated carbon

Many models can be used to calculate pore size distributions, surface areas, and pore volumes. Apart from measuring BET data, we decided to concentrate on methods that provided data that were mutually comparable. The DR (Dubinin–Radushkevich) and the nonlocal DFT (Density Functional Theory) method [12] fulfill this requirement for our samples, and they model slit pores which are indeed present in activated carbon. DR considers a distribution of adsorption energies that depends on the pore size [13]. Nonlocal DFT is based on statistical mechanics including intermolecular potentials of fluid–fluid and fluid–solid interactions; this allows the construction of adsorption isotherms in model pores, and fitting a pore size distribution [12,14,15]. The shape of the DR pore size distribution (single maximum) is consistent with the

DFT result, when only the micropores are considered. When all pore sizes are considered, DFT covers the range from 0.5 nm to 5 nm, which corresponds to relative pressures from  $\sim 7.7 \times 10^{-6}$  to  $\sim 0.7$ . Additionally, Raman spectroscopy yields information on the structural integrity of the carbon.

Porosimetry and Raman spectra recorded after “chemical ageing” indicated no significant changes for the activated carbon powders (data not shown), despite the relatively high temperature of 50 °C and the long immersion time. In contrast, electrochemical ageing had some influence on the microstructure, especially on the pore structure. Fig. 1 and Table 1 present the adsorption characteristics for fresh and aged samples of the three powders A, B and C. The shape of the isotherms is consistent with that from typical microporous materials. The relative volume of the pores in various pore size ranges can be obtained from the histogram, as seen in Fig. 2. In the histograms, we always found a sharp minimum at about 1 nm, which can be attributed to intrinsic shortcomings of the pore model [15–17].

After electrochemical ageing, all three activated carbon powder samples show asymmetric pore structure changes – aged anode powders, i.e. powders polarized positively, suffer more from ageing in terms of surface area, pore volume and micropore volume than aged cathode powders. For aged anode samples, powder B shows the highest porosity loss, while powder C suffers least. Otherwise, the amount of pores in various size ranges does not show significant differences; all powders have a high content of micropores (from 0.5 to 2 nm). Interestingly, already the loss in cathode porosity is higher than the 3% capacitance loss found for complete devices (Epcos ultracaps) after 3000 h ageing at 2.8 V and 30 °C, while the anodic losses we found in the powders are much higher than expected (even considering that we used 2.9 V).

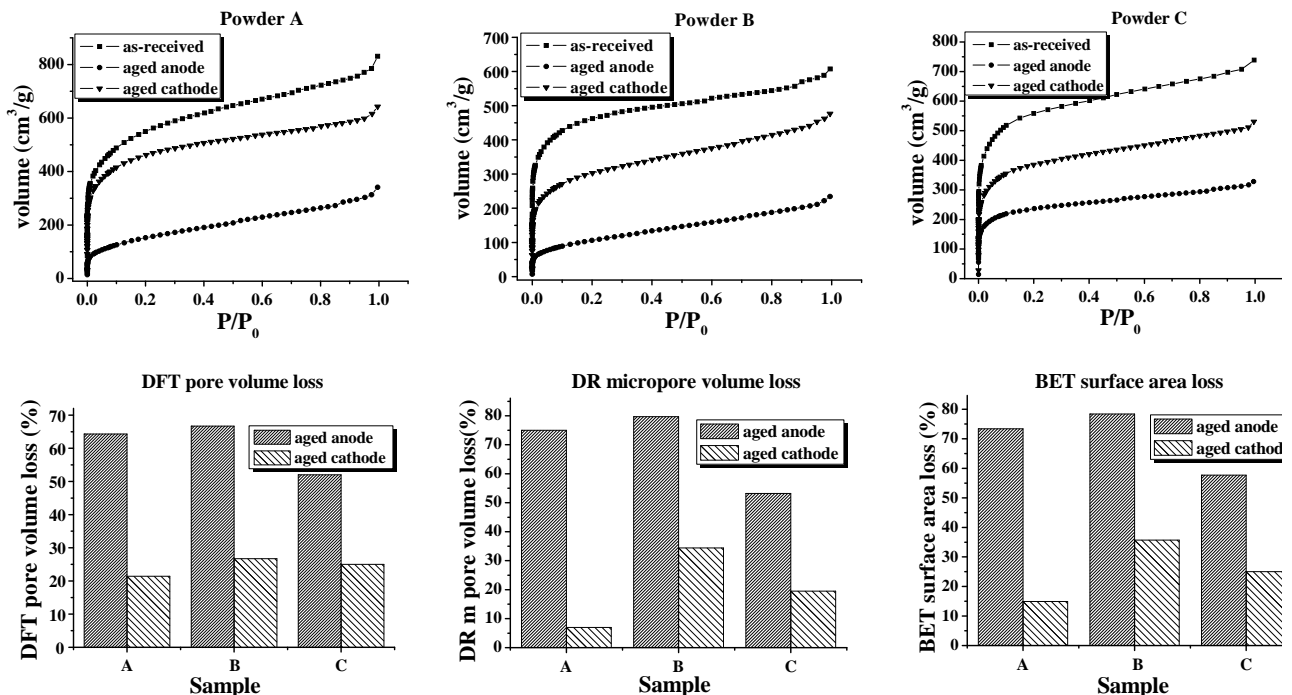


Fig. 1 – Adsorption isotherms and pore volume loss for the three activated carbon powder samples.

**Table 1 – Pore characteristics of the three activated carbon powders A, B and C**

Sample		$S_{\text{BET}}$ ( $\text{m}^2/\text{g}$ )	$S_{\text{DR}}$ ( $\text{m}^2/\text{g}$ )	$V_{\text{mic}}$ ( $\text{cm}^3/\text{g}$ )	$V_{\text{total}}$ ( $\text{cm}^3/\text{g}$ )
A	As received	1988	2015	0.72	0.98
	Aged anode	528	496	0.18	0.35
	Aged cathode	1691	1874	0.67	0.77
B	As received	1721	1812	0.64	0.75
	Aged anode	372	361	0.13	0.25
	Aged cathode	1107	1195	0.42	0.55
C	As received	2101	2182	0.77	0.92
	Aged anode	888	1005	0.36	0.4
	Aged cathode	1580	1732	0.62	0.69

Aged anode means that the carbon has been polarized positively in an electrochemical cell.  
 BET and DR: Brunauer–Emmett–Teller and Dubinin–Radushkevich isotherms; mic: micropores.

It is thus obvious that not all structural changes contribute to real device performance. This merits examining the distribution more closely.

Fig. 2a shows the pore size distribution changes after ageing for powder A. The amount of micropores in aged anodes decreases strongly, which should be the main contribution to the shrinkage of the total adsorption capacity and pore volume. Recently, Lee et al. [18] showed that such processes can be due to immobilization of the  $\text{BF}_4^-$  anion. The content of small mesopores from 2 to 3.2 nm does not show obvious changes, while the amount of mesopores (above 3.2 nm) increases significantly, which might be an effect of the decrease

of the micropore content. Almost the same phenomenon can be found for powder B (Fig. 2b). In contrast, the pore size distribution change on aged cathodes from powder A and B is much less pronounced: Only pores in the size range from 0.5 to 0.8 nm are affected by ageing, which might be due to the spatial confinement of cations ( $(\text{C}_2\text{H}_5)_4\text{N}^+$ ).

Sample C is distinctly different, as seen in Fig. 2c. The pore size distribution does not show the asymmetric change on anode and cathode, and the change of the content of micropores is not as significant. Basically, the pore size distribution is similar to the as-received (fresh) sample. The observation that ageing influences powders A and B more than powder C

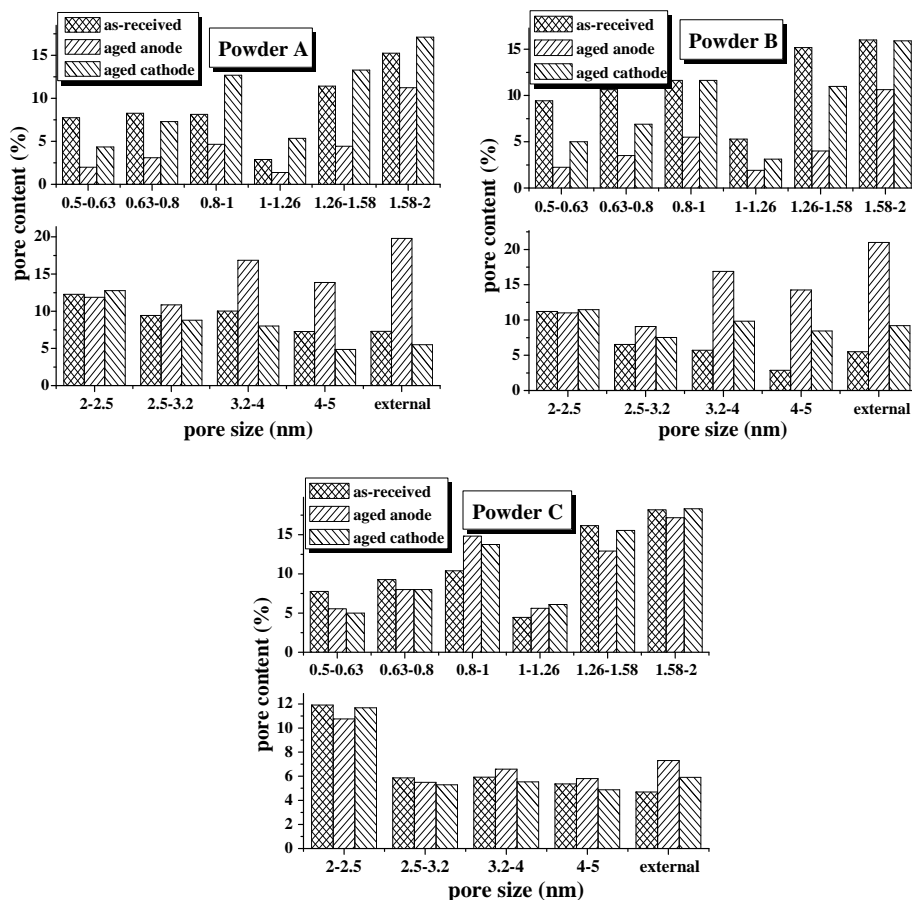
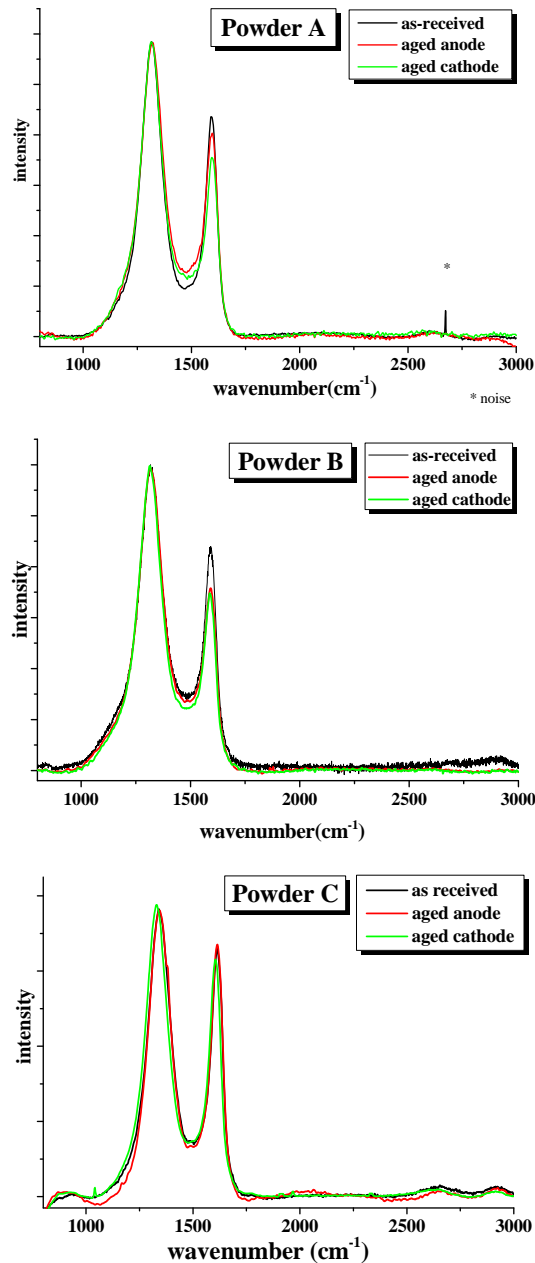


**Fig. 2 – Comparison of the pore size distributions of activated carbons (calculated with the DFT method).**

might be due to the fact that the former two are from natural precursors, while the latter is from a synthetic resin precursor. The greater heterogeneity and impurity (e.g. ash) in natural products is quite likely to cause carbon structures that are more prone to ageing. For example, impurities might act as localized store boxes for water, or lead to local perfor-

mance loss (increased local resistance, closing of pores, etc.).

Our findings are corroborated by Raman spectra of emersed powders (Fig. 3) [19]. The D<sub>1</sub> band indicates the broken symmetry of the disordered graphitic lattice. It remained constant upon ageing. The G band intensity decreased



Wavenumber (cm <sup>-1</sup> )	Assignment
~1200	D <sub>4</sub> band: Disordered graphite, similar to polyaromatic hydrocarbons
1316	D <sub>1</sub> band: Comparable to a breathing mode, broken symmetry
~1500	D <sub>3</sub> band: Amorphous carbon species in activated carbon
1596	G band: C-C stretch
2500-3000	Overtones, combinations: Intact graphite symmetry

Fig. 3 – Raman spectra from fresh and aged activated carbon powder samples; band assignments.

slightly for powders A and B after ageing, a direct consequence of the decrease in content of the ideal graphitic lattice. The  $D_3$  band grew slightly, as expected for the generation of nongraphitic moieties. The weak  $D_4$  band is always present, but shows no clear ageing effects. Powder C shows practically no ageing, more evidence for the higher stability of this material. Powders A and B show the above-mentioned slight, but important changes, that point towards decreasing amounts of graphitic domains.

The results of the microstructural characterization (porosimetry, Raman spectroscopy) after electrochemical ageing indicate that:

- Aged anodes suffer more than aged cathodes in terms of specific area and pore volume.
- For the two activated carbons from natural precursors, the pore size distribution changes significantly after ageing. The micropore content of aged anode powders decreases considerably, compared to fresh and to aged cathode powders.
- The activated carbon from the synthetic resin precursor (powder C) shows better structural stability against ageing, indicated by a smaller decrease of specific area and pore volume of the aged anode powder, and by only minor changes in the pore size distribution.

### 3.2. Chemical changes in activated carbon

We determined the chemical nature of the activated carbon samples after electrochemical ageing (polarization at 2.9 V, negligible current flow) with a range of methods. Note that the quantity of the materials and the homogeneity might vary from sample to sample (i.e., the ageing might depend on the exact location in the compressed powders). Results from the elemental analysis are affected by this, and appear to show results contradictory to those from electrodes. The results have thus to be considered with caution. Hence we do not take the results in this section as quantitative analysis; rather, we aim at a qualitative comparison of anode and cathode from each individual sample.

Elemental analysis results of activated carbon powders are given in Table 2. For the as-received (fresh) samples, “others” means oxygen, which is always available in the carbon material, while aged samples can contain elements such as boron

or fluorine, which originate from electrolyte decomposition [3]. Due to the small amount of paper separator, and due to the dry storage, water from the paper should not play a role in ageing. In real devices, incomplete drying, leaks, and all components (e.g. the separator) can increase the oxygen contents.

From the data, fresh samples have a much higher carbon content than samples used as electrodes. Powder C has—fresh and after ageing—the highest carbon and lowest oxygen content. Again, this supports our assumption that functional groups and composition of activated carbons from synthetic resins can be controlled better than in carbons from natural precursors, and that this improves the stability of the samples. The structural and chemical stability of the powders can be correlated with their purity, which is highest for powder C, and lowest for B. The elemental analysis shows slightly increased nitrogen content on aged anodes. Note that there is practically no nitrogen in the fresh powders. After a careful comparison with the XPS results, which will be shown in the following section, it is clear that chemical shifts of N 1s on aged anodes and aged cathodes are similar, hence we conclude that the (apparent) nitrogen found on aged cathodes is an artifact from mixing the anodically and cathodically aged powders during cell disassembly (see Experimental methods and Supporting information). This means that nitrogen is produced solely on the aged anodes.

Fresh activated carbon powders and electrochemically aged powder samples were measured with XPS. From the survey scans, only oxygen and carbon were found on fresh powders, while fluorine, oxygen, nitrogen and carbon are present on aged anode and aged cathode powders. Note that anodes show much higher nitrogen content than cathodes. The findings suggest presenting a more detailed interpretation for anodes and cathodes, given in the following section.

### 3.3. Aged anodes and cathodes

Fig. 4 shows a typical example of the observed XPS spectra. Peaks pertaining to fluorine, nitrogen, oxygen, and carbon are clearly discernible, except for fluorine and nitrogen species in the fresh powders. Generally speaking, the amount of graphitic carbon at 284.6 eV in all aged anode powders decreased significantly, especially for powder A and powder B. This testifies that new chemical species formed, which result in characteristic energy shifts (Fig. 5, Table 3). For example,

**Table 2 – Elemental analysis results of activated carbons in mol%**

Sample		C	H	N	Others
A	As received	94.6	0.35	0.25	4.8
	Aged anode	71.3	3	11.6	14.1
	Aged cathode	80.4	2.1	6.2	11.3
B	As received	91.8	0.55	0.29	7.4
	Aged anode	67.7	2.7	9	20.6
	Aged cathode	78.5	1.9	4.4	15.2
C	As received	95.7	0.6	0.2	3.5
	Aged anode	67.7	2.6	8.8	20.9
	Aged cathode	83.9	2.5	4.8	8.8

Others refer mainly to oxygen (see XPS results).

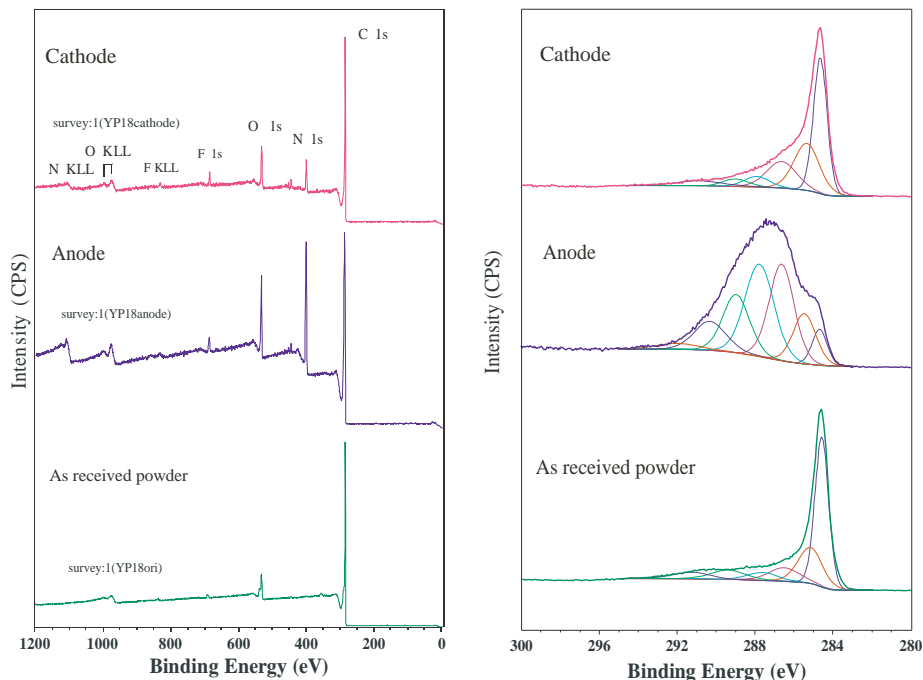


Fig. 4 – XPS spectra of activated carbon (powder sample C) after use in electrodes. Left: survey scans, right: details of the C1s peaks, incl. fit curves.

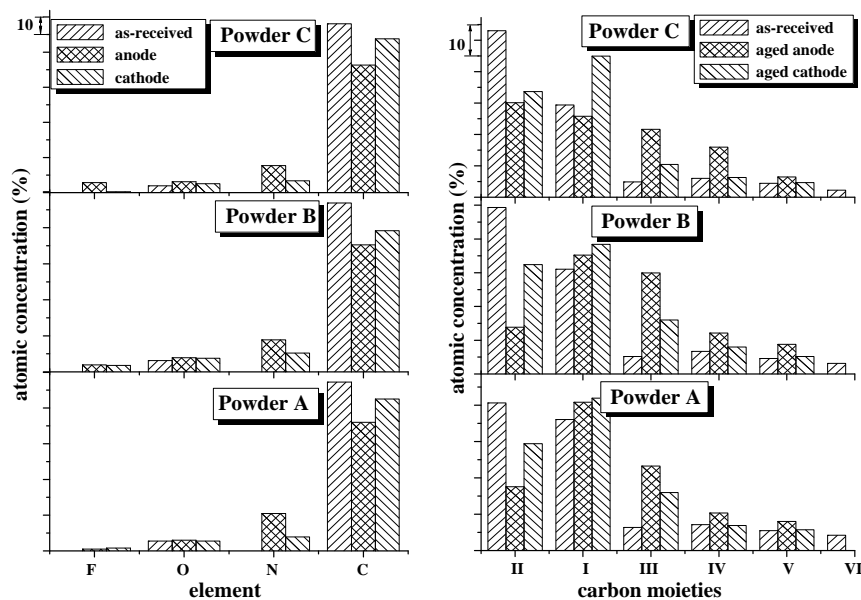


Fig. 5 – XPS results from activated carbons. Left (a): atomic concentration of elements on not aged and aged powders; right (b): atomic concentration of various carbon moieties found on not aged and aged powders, where I = 284.6 eV, II = 285.2 ± 0.3 eV, III = 287 ± 0.3 eV, IV = 288.2 ± 0.3 eV, V = 290 ± 0.3 eV, VI = 291.5 ± 0.3 eV.

the amount of carbon moieties at 285.2 ± 0.3 eV, corresponding to carbon at graphene sheet edges (probably also due to C–H and C–N species, see below), increased on the aged anodes only for powders A and B. It also increased considerably on aged cathodes, possibly due to electrochemical reduction; the hydrogen source is trace water.

The C 1s peaks at higher chemical shifts, corresponding to various C–O and C–N species, increased for all three powder samples. This is corroborated by the O 1s and N 1s signals (Table 4). The O 1s signals merely changed; they can be assigned to carboxylic acids, phenols, and esters (including lactones). In contrast, N 1s signals appeared that had been

**Table 3 – XPS binding energies (C1s) of carbon-based moieties and assignments**

BE (eV)	Assignment
284.6	Graphitic C
285.2 ± 0.3	C–C on the edge of graphene sheets; C–H; C–N
287 ± 0.3	–C=O in quinones and ketones, C–OH, C–O–C; C=N–C
288.2 ± 0.3	–C=O in ketones, carboxylic acids, esters, and amides; C=N–C; CHFCH <sub>2</sub>
290 ± 0.3	O–C=O in carboxylic acids, esters, and amides; π–π* transitions in C
291.5 ± 0.3	Plasmon band in C

**Table 4 – Variation in N 1s, O 1s and F 1s XPS binding energies in activated carbons (comparison of two experiments for each sample)**

Sample	A		B		C	
N 1s						
As received	–	–	–	–	–	–
Aged anode	399.4	400.8	399.5	400.6	399.3	400.6
Aged cathode	399	400.5	399.5	400.6	399.3	400.6
O 1s						
As received	531.8	533.3	531.5	533.2	531.5	533.4
Aged anode	531.5	533	531.8	533.4	531.5	533.5
Aged cathode	531.5	533	531.8	533.1	531.5	533.5
F 1s						
As received	–	–	–	–	–	–
Aged anode	686	688	686.3	688.6	686.3	688.3
Aged cathode	686	688	686.3	688.2	686	688.2

absent in fresh samples. These signals at  $399.3 \pm 0.3$  eV and at  $400.6 \pm 0.3$  eV can be assigned to structures with pyridine moieties (C=N–C), amines (C–NH<sub>2</sub>), polyacetonitrile (–C=N–), and amides (incl. lactams). While oxygen is expected from residual traces of water, covalently bound nitrogen is quite a surprise.

Since no peak in the range of 401–402 eV is observed, which is normally assigned to quaternary nitrogen, the influence from (crystallized and unreacted) electrolyte can be excluded, thus the samples are proven to be washed completely. No boron signal is observed in XPS spectra, so the interference from electrolyte salts can be excluded. The most likely source of nitrogen is the polymerization of the solvent acetonitrile, which would nicely explain also the respective carbon signals (C=N). The polymerization is indeed possible anodically and cathodically. Since boron is absent, the surprising presence of fluorine is due to fluorination of the activated carbon, rather than due to BF<sub>4</sub><sup>–</sup>. However, the fluorine can only stem from the BF<sub>4</sub><sup>–</sup>, which means that the ion is not completely stable. The spectral deconvolution of the F 1s signal shows a peak at about 686 eV, which can be assigned to singly F-substituted carbon structures, and a peak at 688 eV, correlated with doubly or triply fluorinated carbon atoms. This points to a rather aggressive compound, which we did not anticipate. Certainly other anions show much less stability, but one should be aware of these results whenever BF<sub>4</sub><sup>–</sup> is used in long-term applications.

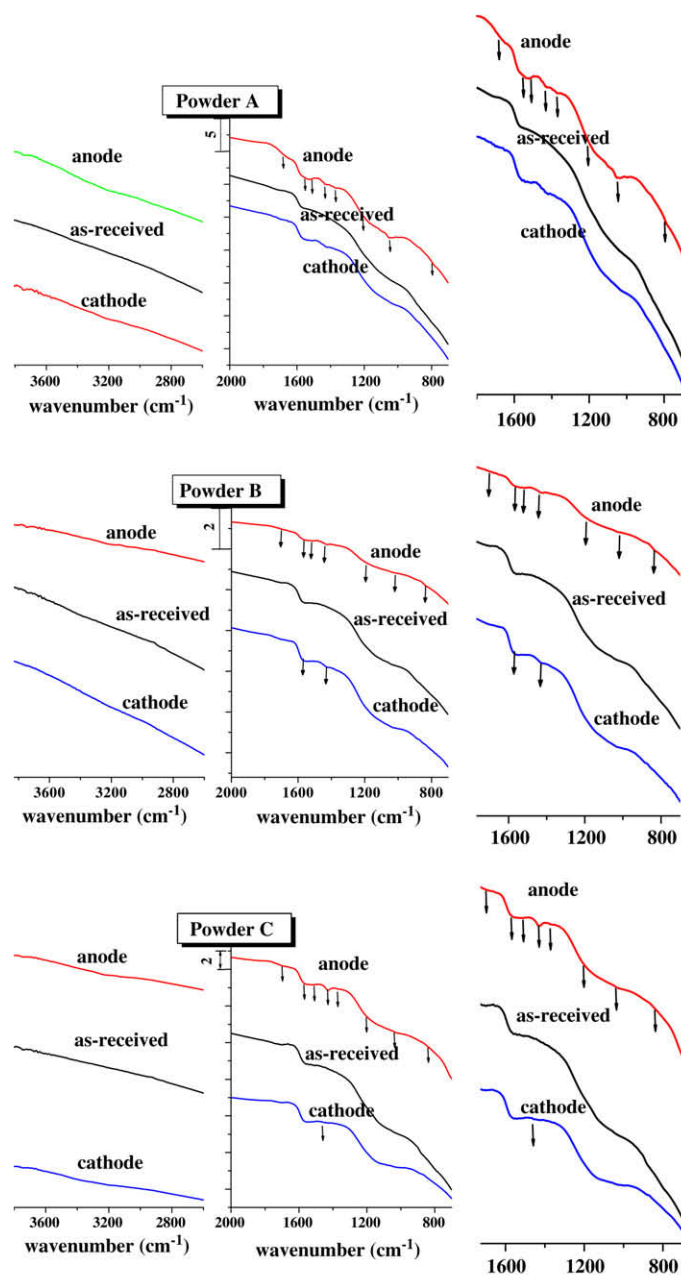
We supported the XPS data by infrared (IR) measurements in the ATR configuration (see Fig. 6 and Supporting information) [20–23]. The principal IR bands are found at  $1580 \text{ cm}^{-1}$  and between  $900$  and  $1300 \text{ cm}^{-1}$ . They can be related to the

presence of oxygen-containing functional groups in the fresh samples. The appearance of new bands after ageing shows the creation of C–H bonds, and the incorporation of oxygen and nitrogen functionalities such as alcohols and amines. The newly appearing bands between  $1750$  and  $1400 \text{ cm}^{-1}$  can be assigned to various C=O and C=N stretching modes, due to covalent binding of oxygen and nitrogen.

Spectra from aged cathode powders show a high similarity with those from fresh powders. Even though the unavoidable mixing of anode and cathode powders during cell disassembly (see Section 2) might affect the results, IR results show very good identification for aged anodes and cathodes, which gives a strong evidence for our presumption that the (apparent) nitrogen on aged cathode powders is from the mixing, but not produced by cathodic processes. Altogether, the agreement with the XPS data is good. This means that the much faster and cheaper infrared spectroscopy can replace the complex XPS method at least for routine analyses as required for quality control. As mentioned above, Epcos ultracaps, aged for 3000 h at 2.8 V lose only 3% of their capacitance, hence our conditions likely correspond to forced ageing in short times, a good test for determination of suitable materials.

In conclusion we can state:

- On fresh powders, only small amounts of oxygen species exists, mainly in the form of quinoids, ketones and ethers.
- The presence of unwanted and even unexpected chemical reactions (resulting in nitrogen and fluorine moieties) means that, different from standard electrochemical considerations, one has to allow for the extremely slow kine-



Wavenumber (cm <sup>-1</sup> )	Assignment
900-1300	C-O stretch (ethers, esters, phenols); C-H bend in aromatic systems
1340-1370	O-H deformation; C-N, C-O stretch
1400-1460	C-OH bend; C-N-H bend in amides; C-H deformation; aromatic C-C stretch
1540	C-N-H stretch-bend in amides
1580	C-C stretch in polyaromatic quinoids
1600-1750	C=O stretch in carbonyls, C=N stretch
3000-3600	O-H stretch, N-H stretch (C-H stretch only below 3150 cm <sup>-1</sup> )

Fig. 6 – IR spectra of activated carbons and assignment table. At right: Enlarged parts. The arrows highlight vibrations in chemical groups that are formed by ageing.

tics of these processes; hence usually not observed reactions can occur. The tendency of all chemical systems to move towards thermodynamical equilibrium manifests for our very long ageing times.

- Anodic ageing produces nitrogen-containing species, including pyridine moieties ( $-\text{C}=\text{N}-\text{C}-$ ), amines ( $\text{C}-\text{NH}_2$ ), polyacetonitrile, amides, all covalently linked to graphene sheets. The most likely reaction is anodic and cathodic polymerization of acetonitrile.
- After ageing, more oxygen moieties are formed, such as phenol, carboxylic acid, esters (lactones), on both aged anode and cathode. The decomposition of the anion leads to the surprising formation of covalent C-F bonds at anodes and cathodes.
- XPS results indicate that more carbon has to be attributed to nongraphitic carbon after ageing (at graphene edges or from newly formed chemical groups). This is especially true for aged cathode powders, in other words, the cathode is reduced. The hydrogen can originate from residual water or from the decomposition of the cation. Certainly such reactions must have an influence on the microstructure, which is shown by the porosimetry (reduced internal volume), and Raman experiments (disorder).

#### 4. Results for conductive agents (carbon blacks)

Carbon black is added to device electrodes in relatively low concentration to improve the conductivity (hence to lower

the equivalent series resistance). Its structural and chemical stability should be higher than that of activated carbon. We tested an acetylene carbon black sample (A-B), and two Ketjen blacks, K-A and K-B. Considerable influences on the ageing are not expected, and one would rather focus on activated carbon and on further ingredients such as binders [11] and additives. However, we found that data from experiments conducted in the same manner as for activated carbon are valuable to confirm the expectations, and to contrast the findings for activated carbons.

##### 4.1. Microstructural characterization

The Raman spectrum of the fresh acetylene carbon black A-B shows a clear band at  $2660\text{ cm}^{-1}$  (see Fig. 7), which is the overtone of the  $\text{D}_1$  band at  $1320\text{--}1350\text{ cm}^{-1}$  discussed before (see Fig. 3). Hence the sample contains a large amount of well-ordered graphite, while defects would create  $\text{sp}^3$  bonds that reduce the band intensity [24]. The band intensity decreases on both electrodes (Fig. 7), and this observation is also well reproducible for chemically aged A-B. This might be due to  $\text{sp}^3$  bonds, but also due to intercalation of small molecules or ions, causing expansion of the lattice, as found for supercapacitor electrodes [18].

##### 4.2. Chemical characterization

Elemental analysis results are given in Table 5. The influence from ageing on the conductive agents is not pronounced: A-B shows practically no, and K-B only slight changes. In contrast,

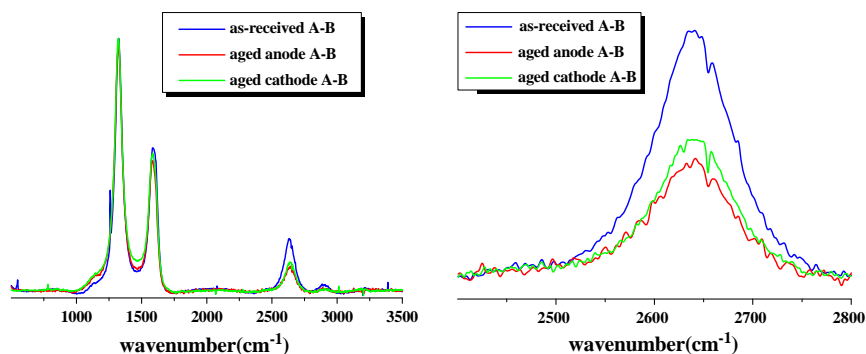
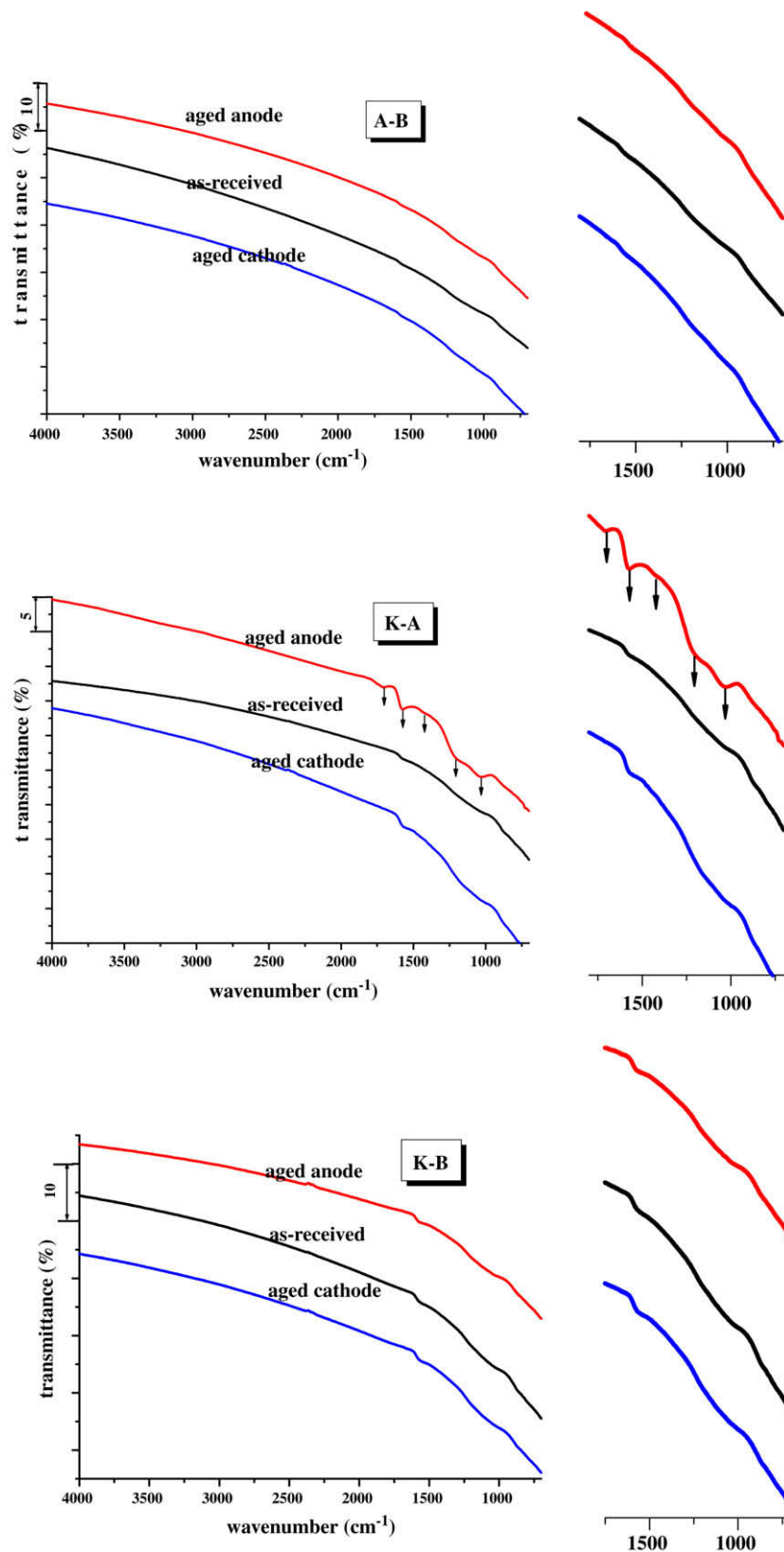


Fig. 7 – Raman spectra of carbon black A-B. Ageing results in small, but clearly visible structural changes.

Table 5 – Elemental analysis results of conductive agents (carbon blacks)

Sample		C	H	N	Others
A-B	As received	99	–	–	1
	Aged anode	99.3	–	–	0.7
	Aged cathode	99	–	–	1
K-A	As received	93.5	0.8	0.2	4.5
	Aged anode	75.5	1.5	2.3	20.7
	Aged cathode	89.4	1.7	1.4	7.5
K-B	As received	93.5	0.7	0.3	4.5
	Aged anode	93.5	0.9	0.9	4.7
	Aged cathode	93.3	0.9	0.7	5.1

A-B: acetylene black, K-A: Ketjen black A, K-B: Ketjen black B.



**Fig. 8** – IR spectra of the three conductive agents (carbon blacks). At right: Enlarged parts. The arrows highlight vibrational bands of chemical groups that are formed by ageing.

K-A is oxidized: We find increased amounts of oxygen and nitrogen. The IR spectra of the three conductive agents

(Fig. 8) provide more details. The band positions are similar to what we observed on activated carbons, while the relative

intensity of the bands is lower, which means that fewer functional groups are present. Again, A-B and K-B exhibit no observable changes, and should thus be preferred. Parallel to the elemental analysis, the IR spectrum of the aged K-A anode is much different from that of fresh K-A and cathodically aged K-A, and is reminiscent of the spectra from anodically activated carbon powders: The newly emerging bands point towards formation of functional groups based on carbonyl and C=N species. Cathodic ageing of K-A produces only very slight changes.

In conclusion, the relatively simple and fast IR spectra might be used as indicator for choosing conductive agents, here pointing out potential problems with the use of K-A. The results from elemental analysis and IR of the conductive agents give evidence for the assumption we made before: Oxygen functional groups in the carbonaceous materials can promote ageing processes on anodes and cathodes that result here not in considerable loss of porosity, but in chemical changes. The ageing effects on conductive agents are quite small, but they demonstrate that Acetylene black A-B has lower oxygen content than the Ketjen blacks. Ageing obviously causes microcrystallinity changes in acetylene black, while influences on Ketjen blacks are small. The microcrystallinity change is here, different from activated carbon, mainly attributable to the size of the graphene sheets, and purely physical. Altogether, acetylene black has the best chemical stability, owing to its high purity. The changes in its microstructure are obvious, but so small that they do not manifest in enhanced chemical reactivity.

## 5. Conclusions

The ageing of carbon materials in acetonitrile-based electrolyte is very slow, and even under conditions of forced ageing (increased electrochemical potential) at least several weeks are required to produce measurable changes. From Raman and nitrogen porosimetry data, we attribute these changes to structural defects, i.e. micro- and mesopores are destroyed or closed, which can for a large part be attributed to the polymerization of acetonitrile at anodes and cathodes. A meaningful chemical analysis is only possible when a range of methods is combined; especially XPS (see also [3,4]) and infrared spectroscopy turned out to be useful. Depending on absence or presence of electrolyte, and on the use of pure materials or assembled electrodes, the carbon is chemically altered to various degrees. The alteration shows pronounced dependence on the polarity, i.e. cathodes age much slower than anodes. This finding should lead to new design considerations in supercapacitors, e.g. thicker anodes in an asymmetric design to make up for the loss of capacitance, or in the case of temperature gradients, placing the anode in a colder environment. The most important changes amount to formation of C–H bonds on the cathode (reduction), and C–N and C–F bonds especially on the anode, likely due to the polymerization of acetonitrile, which also works cathodically, and due to the unusual and unexpected decomposition of tetrafluoroborate. The practically unavoidable presence of water traces is of great importance for nearly all “chemical ageing” processes, providing oxygen and hydrogen, and thus producing some C–O species.

## Acknowledgements

We are grateful to Dr. Shengfa Ye and Mrs. B. Förtsch, Universität Stuttgart, for assistance with the chemical analyses, and to Prof. Dr. H. Vogt and Mr. A. Schulz for help with Raman spectroscopy. We thank Dr. H.-F. Waibel for help in the beginning stages of the project and P. Azais for helpful discussions. We thank Epcos AG, Heidenheim, Germany, where CJW was employed during the time this work has been accomplished.

## Appendix A. Supplementary material

Supplementary data associated with this article can be found, in the online version, at [doi:10.1016/j.carbon.2008.07.025](https://doi.org/10.1016/j.carbon.2008.07.025).

## REFERENCES

- [1] Conway BE. *Electrochemical supercapacitors: Scientific fundamentals and technological applications*. New York: Kluwer Academic/Plenum Publisher; 1999.
- [2] Kötzt R, Carlen M. *Electrochim Acta* 2000;45:2483.
- [3] Aza P. *Causes of ageing of supercapacitors based on activated carbon electrodes and organic electrolyte*. Ph. D dissertation. France: Orléans; 2003.
- [4] Aza P, Duclaux L, Florian P, Massiot D, Lillo-Rodenas M-A, Linares-Solano A, et al. *J Power Sources* 2007;171:1046.
- [5] Hahn M, Würsig A, Gallay R, Novák P, Kötzt R. *Electrochem Commun* 2005;7:925.
- [6] Winter M, Brodd RJ. *Chem Rev* 2004;104:4245.
- [7] Bansel RC, Donnet J-B, Stoeckli F. *Active carbon*. New York: Marcel Dekker; 1988.
- [8] Franklin R. *Proc R Soc London Ser A* 1951;209:196.
- [9] Byrne JF, Marsh H. *Introductory overview*. In: Patrick JW, editor. *Porosity in carbons: Characterisation and applications*. London: Arnold; 1995. p. 1.
- [10] Pikunic J, Clinard C, Cohaut N, Gubbins KE, Guet J-M, Pellenq R-J-M, et al. *Langmuir* 2003;19:8565.
- [11] Richner R, Müller S, Bärtschi M, Kötzt R, Wokaun A. *J New Mat Electrochem Systems* 2002;5:297.
- [12] Jagiello J, Ania CO, Parra JB, Jagiello L, Pi JJ. *Carbon* 2007;45:1066.
- [13] Dubinin MM, Radushkevich LV. *Dokl Akad Nauk SSR* 1947;55:331.
- [14] Cracknell RF, Gubbins KE, Maddox M, Nicholson D. *Acc Chem Res* 1995;28:281.
- [15] Jagiello J, Thommes M. *Carbon* 2004;42:1227.
- [16] Jagiello J, Tolles D. In: Meunier F, editor. *Fundamentals of adsorption*. Amsterdam: Elsevier; 1998. p. 629.
- [17] Olivier JP. Paper presented at the 1997 AIChE annual meeting. Los Angeles; 1997.
- [18] Lee S-I, Saito K, Kanehashi K, Hatakeyama M, Mitani S, Yoon S-H, et al. *Carbon* 2006;44:2578.
- [19] Mapelli C, Castiglioni C, Meroni E, Zerbi G. *J Mol Struct* 1999;480–481:615.
- [20] Biniak S, Szymanski G, Siedlewski J, Swiatkowski A. *Carbon* 1997;35:1799.
- [21] Figueiredo JL, Periera MFR, Freitas MMA. *Carbon* 1999;37:1379.
- [22] Socrates G. *Infrared characteristic group frequencies*. 3rd ed. Chichester, England: Wiley & Sons; 2000.
- [23] Lin-Vien D, Colthup NB, Fateley WG, Grasselli JG. *The handbook of infrared and Raman characteristic frequencies of organic molecules*. Academic Press; 1991.
- [24] Tan PH, Dimovski S, Gogotsi Y. *Phil Trans Royal Soc Lond A* 2004;362:2289.